

Rapid compensatory evolution can rescue low fitness symbioses following partner switching

Highlights

- Partner-switches show intergenomic epistasis in the *Paramecium-Chlorella* symbiosis
- Low fitness host-symbiont pairings show elevated symbiont stress metabolites
- Poorly performing pairings rapidly gain higher fitness by compensatory evolution
- Compensatory evolution could arise by either host or symbiont adaptation

Authors

Megan E.S. Sørensen, A. Jamie Wood, Duncan D. Cameron, Michael A. Brockhurst

Correspondence

michael.brockhurst@manchester.ac.uk

In brief

Sørensen et al. show that partner switching of symbionts creates phenotypic novelty for hosts but that low fitness pairings are associated with elevated symbiont stress. Poorly performing pairings increase fitness by compensatory evolution of host or symbiont. Combined, these processes will enable symbioses to respond to changing environments.

Article

Rapid compensatory evolution can rescue low fitness symbioses following partner switching

Megan E.S. Sørensen,¹ A. Jamie Wood,² Duncan D. Cameron,¹ and Michael A. Brockhurst^{3,4,5,*}

¹Department of Animal and Plant Sciences, University of Sheffield, Sheffield S10 2TN, UK

²Department of Biology, University of York, York YO10 5DD, UK

³Division of Evolution and Genomic Sciences, School of Biological Sciences, University of Manchester, Manchester M13 9PT, UK

⁴Lead contact

⁵Twitter: @BrockhurstLab

*Correspondence: michael.brockhurst@manchester.ac.uk

<https://doi.org/10.1016/j.cub.2021.06.034>

SUMMARY

Partner switching plays an important role in the evolution of symbiosis, enabling local adaptation and recovery from the breakdown of symbiosis. Because of intergenomic epistasis, partner-switched symbioses may possess novel combinations of phenotypes but may also exhibit low fitness due to their lack of recent coevolutionary history. Here, we examine the structure and mechanisms of intergenomic epistasis in the *Paramecium-Chlorella* symbiosis and test whether compensatory evolution can rescue initially low fitness partner-switched symbioses. Using partner-switch experiments coupled with metabolomics, we show evidence for intergenomic epistasis wherein low fitness is associated with elevated symbiont stress responses either in dark or high irradiance environments, potentially owing to mismatched light management traits between the host and symbiont genotypes. Experimental evolution under high light conditions revealed that an initially low fitness partner-switched non-native host-symbiont pairing rapidly adapted, gaining fitness equivalent to the native host-symbiont pairing in less than 50 host generations. Compensatory evolution took two alternative routes: either hosts evolved higher symbiont loads to mitigate for their new algal symbiont's poor performance, or the algal symbionts themselves evolved higher investment in photosynthesis and photoprotective traits to better mitigate light stress. These findings suggest that partner switching combined with rapid compensatory evolution can enable the recovery and local adaptation of symbioses in response to changing environments.

INTRODUCTION

Beneficial symbioses have an inherent potential for conflict between the symbiotic partners. This can drive the breakdown of symbiosis if environmental conditions change the net benefit of interacting or if the pursuit of individual fitness favors cheating.¹ Both situations can select for partner switching to recombine symbiotic partnerships.² Partner switching can provide hosts with access to favorable symbiotic phenotypes to overcome maladaptation to the prevailing environmental context³ or restore symbiont function following breakdown.^{4,5} The generation of phenotypic plasticity through partner switching arises from genetic variation of hosts (G^H) and symbionts (G^S) and intergenomic epistasis,⁶ that is, genetic variation for the outcome of symbiosis in the form of host genotype by symbiont genotype interactions ($G^H \times G^S$) for symbiotic traits or fitness. Furthermore, the fitness effects of symbiosis can be mediated by the environmental context,⁷ causing host-genotype-by-symbiont-genotype-by-environment interactions ($G^H \times G^S \times E$). A consequence of $G^H \times G^S \times E$ interactions is that there is unlikely to be an optimal host-symbiont pairing across all environments,

further driving selection for partner switching or dynamic coevolution of the symbiosis.⁸ As such, partner switching can enable niche expansion by hosts^{9,10} and provide a mechanism by which hosts can adapt to local environmental conditions faster than through *de novo* adaptation of the current symbiont.^{11,12}

Newly interacting partner-switched host-symbiont pairings are, however, unlikely to be co-adapted due to their lack of recent coevolutionary history and may, therefore, initially have low fitness.^{13–15} Indeed, despite the adaptive potential of partner switching, new host-symbiont pairings, like genetic mutations, may more often be deleterious than beneficial to host fitness due to phenotypic mismatches or genetic incompatibilities. This has been observed in a range of symbiotic interactions: for example, a newly acquired *Symbiodinium* endosymbiont was found to translocate less fixed carbon than the native symbiont to its cnidarian host¹³; novel bacterial endosymbionts had reduced vertical transmission rates in aphid hosts,¹⁴ and novel *Wolbachia* endosymbionts reduced the reproductive fitness of *Drosophila simulans*.¹⁵ How then do newly formed, poorly co-adapted host-symbiont pairings become stable, beneficial symbioses? We hypothesize that rapid compensatory evolution (that

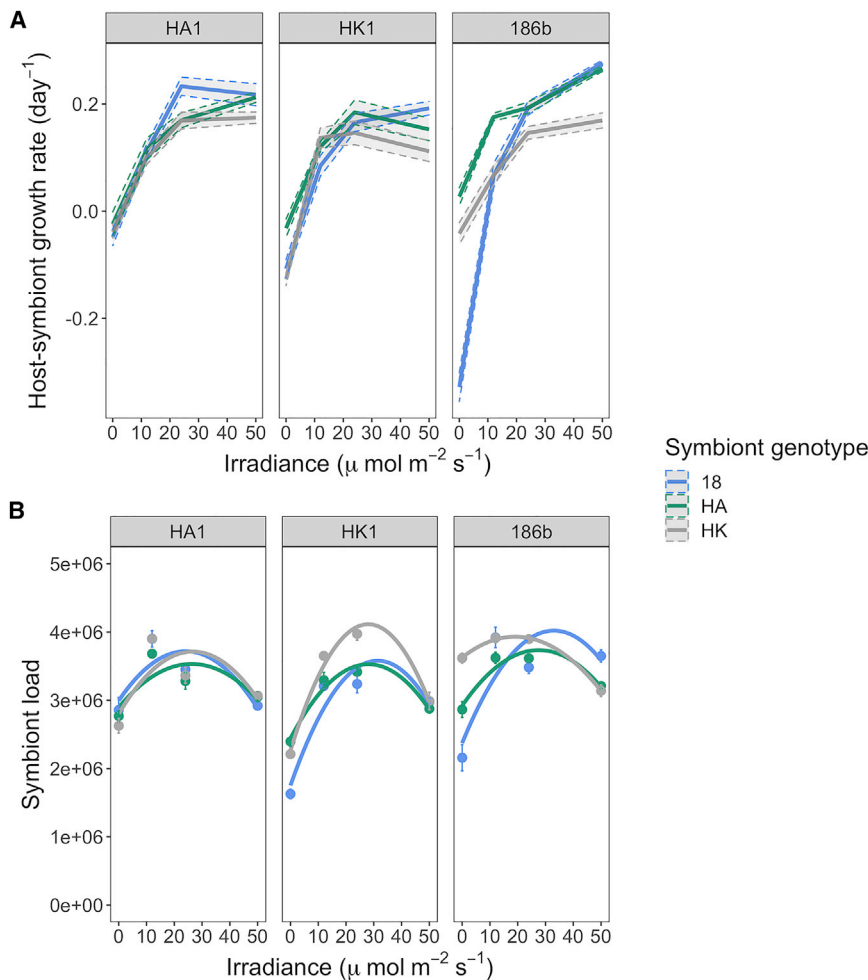


Figure 1. Intergenomic epistasis of host-symbiont growth rate and symbiont load reaction norms

For both (A) and (B), each panel presents the data for a specific genotype of *P. bursaria* host, as indicated at the top of each panel, and the symbiont genotypes are distinguished by color.

(A) Initial growth rates of the host-symbiont pairings across a light gradient over 3 days. The data points show the mean (n = 3) initial growth rate \pm SE. The host-symbiont growth rate reaction norm varied by symbiont genotype in the 186b host genotype but did not vary in the HA1 or HK1 host genotypes, consistent with intergenomic epistasis.

(B) Symbiont load of the host-symbiont pairings across a light gradient. The data points show the mean (n = 3) symbiont load, measured as relative chlorophyll fluorescence, \pm SE. The lines show polynomial models; the model coefficients showed a significant $G^H \times G^S$ interaction (ANOVA, $F_{8,36} = 27.22$ (the intercept); 8.58 (first coefficient); 6.09 (second coefficient), $p < 0.001$). For full statistical output, see [Data S1](#). The symbiont load reaction norm varied by symbiont genotype in both the HK1 and 186b host genotypes but did not vary in the HA1 host genotype, consistent with intergenomic epistasis. Related to [Figure S2](#), [Data S1](#), and [Table S1](#).

geographically widespread and genetically diverse, in part, due to multiple independent acquisitions of algal symbionts by *P. bursaria*. The primary nutrient exchange is convergent among these origins.²³ This facilitates partner switching, but concurrent divergence in other meta-

is, adaptation of the host, the symbiont, or both to ameliorate the deleterious fitness effects of partner switching) could allow partner-switched symbioses to overcome their initially low fitness. Indeed, there is some, albeit limited, experimental evidence to support this idea: for example, the high fitness cost of newly acquired *Spiroplasma* endosymbionts in *Drosophila melanogaster* was ameliorated within only 17 host generations,¹⁶ although the underlying mechanisms of this fitness recovery remain unknown. Furthermore, horizontal gene transfers were found to have caused the rapid evolution of nonsymbiotic strains of rhizobia bacterial symbionts into symbiotic partners in field-site tests with *Lotus* plant hosts.¹⁷

The microbial symbiosis between *Paramecium bursaria* and *Chlorella* provides an experimentally tractable model system to study intergenomic epistasis and the underlying molecular mechanisms. The ciliate host, *P. bursaria*, is a single-celled eukaryote, and each host cell contains 100–600 cells of the algal endosymbiont, *Chlorella*.^{18,19} The *P. bursaria* - *Chlorella* symbiosis is based on a primary nutrient exchange of fixed carbon from the photosynthetic alga for organic nitrogen from the heterotrophic host.^{18,20} *Chlorella* algal symbionts are primarily vertically transmitted to daughter cells at *Paramecium* cell division, although additional algal symbionts can also be acquired from the environment by ingestion.^{21,22} This symbiosis is

metabolic traits can cause phenotypic mismatches in partner-switched host-symbiont pairings.²³ Here, using experimental partner switches, we examined the pattern and mechanisms of intergenomic epistasis for three diverse host-symbiont strains, observing significant $G^H \times G^S \times E$ interactions for host-symbiont growth rate and symbiont load (that is, the number of symbionts per host cell), together with corresponding differences in metabolism. We then experimentally evolved a low fitness partner-switched host-symbiont pairing for \sim 50 host generations. We observed rapid compensatory evolution by hosts and symbionts that improved fitness to equal to that of the native host-symbiont pairing, mediated by evolved changes in host control of symbiont load and in symbiont metabolism.

RESULTS

Intergenomic epistasis for host-symbiont growth and symbiont load

We constructed all possible host-symbiont genotype pairings (n = 9) of 3 diverse strains of *Paramecium-Chlorella* and confirmed their identity by diagnostic PCR ([Figure S1](#)). We measured the growth reaction norm of each host-symbiont pairing across a light gradient ([Figure 1A](#)). All host-symbiont pairings showed the classic photosymbiotic reaction norm²⁴, such that

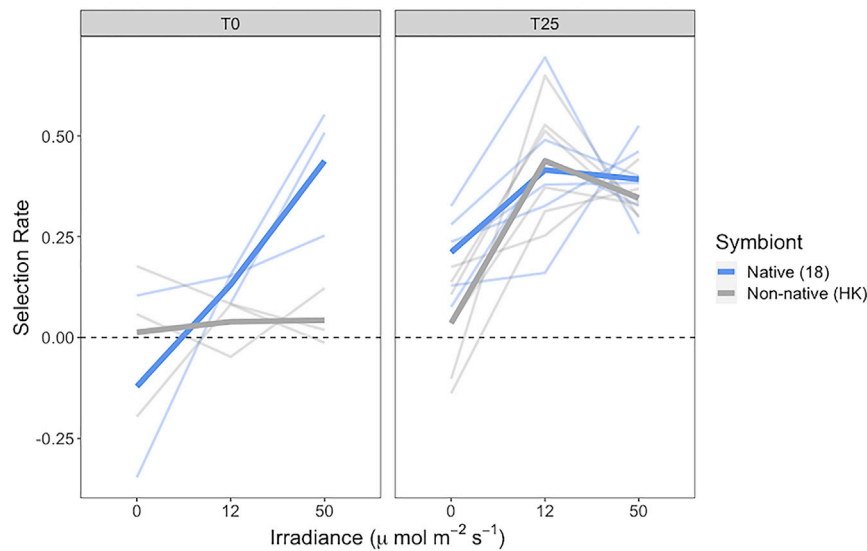


Figure 2. Relative fitness reaction norms at the start and end of the evolution experiment

Panels show relative fitness reaction norms across a light gradient of various host-symbiont pairings in the 186b host genotype in direct competition with the symbiont-free 186b host genotype. The left-hand panel shows fitness reaction norms measured at the start of the evolution experiment (T0), and the right-hand panel shows fitness reaction norms measured at the end of the evolution experiment (T25), as indicated at the top of each panel. Relative fitness was calculated as the selection rate, where a value above 0 indicates a fitness benefit to the host of carrying algal symbionts. Colors show the symbiont genotype treatment, where blue denotes that the 186b host carried the native 186b symbiont genotype, whereas gray denotes that the 186b host carried the non-native HK1 symbiont genotype. Dark, thick lines show the mean ($n = 6$) relative fitness reaction norms, and light, thin lines show the relative fitness reaction norms for each individual replicate. At the

start of the evolution experiment, only the native host-symbiont pairing showed an increasing fitness benefit of carrying symbionts with increasing irradiance, whereas at the end of the evolution experiment both the native and non-native host symbiont pairings showed an increasing fitness benefit of carrying symbionts with increasing irradiance. Related to [Figure S3](#) and [Data S1](#).

growth rate increased with irradiance, but we observed a significant $G^H \times G^S \times E$ interaction for host-symbiont growth rate ($G^H \times G^S \times E$ interaction, ANOVA, $F_{17,162} = 18.81$, $p < 0.001$) consistent with intergenomic epistasis. This was driven by contrasting effects of symbiont genotype on growth in the different host backgrounds across light environments. In the HK1 and HA1 host backgrounds, similar growth reaction norms were observed for each symbiont genotype, whereas in the 186b host background the growth reaction norm varied according to symbiont genotype. Interestingly, the native 186b host-symbiont pairing had both the lowest intercept and the highest slope, indicating that in the 186b host background the native algal symbiont genotype was costlier in the dark (Welch t test on native versus non-native symbionts $t(7.29) = -10.13$, $p < 0.001$) yet more beneficial in high-light environments than non-native algal symbiont genotypes (Welch t test on native versus non-native symbionts $t(10.44) = 3.21$, $p < 0.01$).

P. bursaria host cells regulate their algal symbiont load (i.e., the number of symbionts per host cell) according to light irradiance to maximize the benefit-to-cost ratio of symbiosis, such that, for naturally occurring host-symbiont pairings, symbiont load peaks at intermediate irradiance and is reduced both in the dark and at high irradiance.^{24–26} To test whether regulation of symbiont load varied among host-symbiont pairings, we measured symbiont load across the light gradient as the intensity of single-cell fluorescence, which is correlated with the number of symbionts per host cell,¹⁹ by flow cytometry (Figure 1B). All host-symbiont pairings showed the expected unimodal symbiont load curve with light, but nevertheless we observed a significant $G^H \times G^S \times E$ interaction for symbiont load ($G^H \times G^S \times E$ interaction, ANOVA, $F_{17,162} = 3.78$, $p < 0.001$) consistent with intergenomic epistasis. Whereas, in the HA1 host similar symbiont load reaction norms were observed for each symbiont genotype, for the HK1 and 186b host backgrounds the form of the symbiont load reaction norms varied according to symbiont genotype. In

the HK1 host, the magnitude of the symbiont load varied by symbiont genotype, such that higher symbiont loads were observed for the native compared to the non-native symbiont genotypes. In the 186b host, peak symbiont load occurred at different light levels according to symbiont genotype, such that for the native symbiont the symbiont load curve peaked at a higher light intensity when compared to the non-native symbionts. (For the full output of the polynomial model, see [Data S1](#).) Because symbiont load is primarily host controlled in this system,^{24,25} this suggests that the HK1 and 186b host genotypes discriminated among symbiont genotypes and then regulated symbiont load accordingly.

Metabolic mechanisms of intergenomic epistasis

To investigate the potential metabolic mechanisms underlying the observed intergenomic epistasis, we performed untargeted global metabolomics with ESI-ToF-MS independently for the host and symbiont metabolite fractions for each host-symbiont pairing across the light gradient.²³ Light irradiance was the primary driver of differential metabolism for both host and symbiont; however, host-dependent differences in the metabolism of symbiont genotypes could be detected. For the symbiont metabolite fraction subset by host genotype, we observed native versus non-native clustering of symbiont metabolism only when associated with the 186b host genotype (Figure S2). This is consistent with the larger phenotypic differences in growth and symbiont load observed among host-symbiont pairings with the 186b host genotype compared to with either the HK1 or HA1 host genotypes. We therefore focused our analyses on comparing the metabolic profiles of the different symbiont genotypes within the 186b host background. Pairwise contrasts of the symbiont genotypes in the 186b host genotype background revealed a range of candidate symbiont metabolites that distinguished the native pairing from either non-native host-symbiont pairing. Putative identifications included, in the dark, elevated

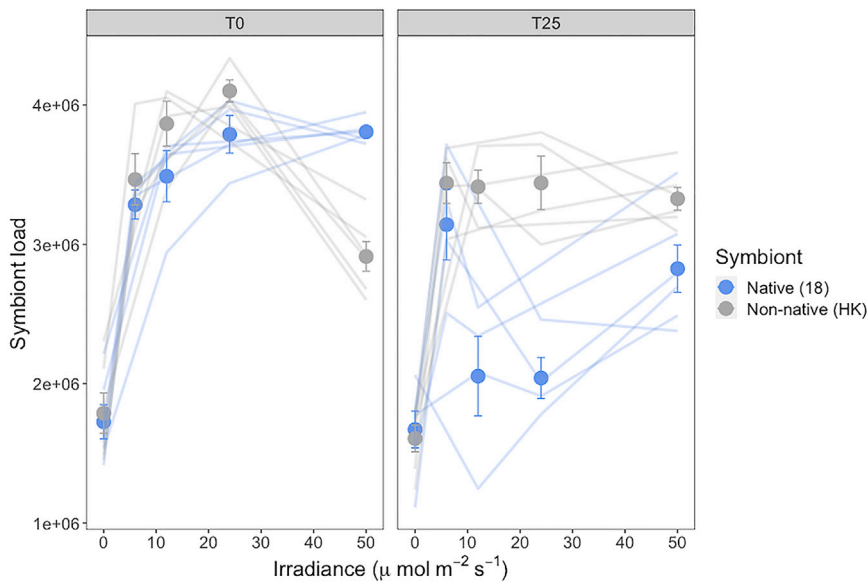


Figure 3. Symbiont load reaction norms at the start and end of the evolution experiment

Panels show symbiont load reaction norm across a light gradient of various host-symbiont pairings in the 186b host genotype. The left-hand panel shows symbiont load reaction norms measured at the start of the evolution experiment (T0), and the right-hand panel shows symbiont load reaction norms measured at the end of the evolution experiment (T25), as indicated at the top of each panel. Colors show the symbiont genotype treatment, where blue denotes that the 186b host carried the native 186b symbiont genotype, whereas gray denotes that the 186b host carried the non-native HK1 symbiont genotype. Symbols show the mean ($n = 6$) \pm SE symbiont load and lines show the symbiont load reaction norms for each individual replicate. At the irradiance level used in the evolution experiment ($50 \mu\text{E m}^{-2} \text{s}^{-1}$), we observed that, whereas mean symbiont load of the native symbiont had reduced, symbiont load of the non-native symbiont had increased, by the end of the evolution experiment. Related to [Figure S3](#), [Data S1](#), and [Table S3](#).

levels of candidate metabolites associated with stress responses (stress-associated hormones, jasmonic acid and abscisic acid, and stress associated-fatty acids, such as arachidonic acid) but reduced production of vitamins and co-factors by the native symbiont, compared to the non-native symbionts ([Table S1](#)). At high irradiance, the native symbiont showed higher levels of candidate metabolites in central metabolism, hydrocarbon metabolism, and of biotin (vitamin B7), compared to the non-native symbionts ([Table S1](#)). In contrast, the non-native symbionts produced elevated levels, relative to native symbionts, of a candidate glutathione derivative; glutathione is an antioxidant involved in the ascorbate-glutathione cycle that combats high UV stress through radical oxygen scavenging.^{27,28} Together, these data suggest that impaired host-symbiont performance was associated with elevated symbiont stress responses and that symbiont genotypes varied in their requirement for host photoprotection, providing a putative mechanism underlying inter-genomic epistasis.

Rapid compensatory evolution can rescue an initially low fitness partner-switched symbiosis

The partner-switched pairing of the 186b host with the HK1 symbiont showed substantially reduced growth at high light relative to the native 186b host-symbiont pairing. To test whether this fitness deficit could be overcome through compensatory evolution, we established six replicate populations of each of these two symbiotic partnerships (i.e., the 186b host with the 186b algal symbiont and the 186b host with the HK1 algal symbiont), which were propagated by weekly serial transfer for 25 transfers (approximately 50 host generations) at a high light regime ($50 \mu\text{E}$; 14:10 L:D). The growth rate per transfer was higher for the native pairing than the non-native pairing ([Figure S3A](#)) (linear mixed effect model, HK1 symbiont fixed effect of -0.08 ± 0.006 , T-value = -14.126 , see [Data S1](#) for full statistical output) but increased over time for both pairings (transfer number fixed effect 0.001 ± 0.0004 , T-value = 3.088). To test for adaptation, we

compared the fitness effect of symbiosis at the beginning and the end of the transfer experiment by direct competition of either the ancestral or evolved host-symbiont pairings against the symbiont-free ancestral 186b host genotype across a light gradient. Fitness at the start of the evolution experiment of symbiotic relative to non-symbiotic hosts increased more steeply with irradiance for the native than the partner-switched non-native pairing ([Figure 2](#)), but this difference had disappeared by the end of the evolution experiment, such that both the native and non-native host-symbiont pairings showed increasing fitness relative to non-symbiotic hosts with increasing irradiance (symbiont genotype by light intensity by transfer number interaction term: ANOVA, $F_{7,45} = 6.20$, $p < 0.001$). Indeed, at $50 \mu\text{E m}^{-2} \text{s}^{-1}$, the light level used in the selection experiment, the large fitness deficit observed between the native and non-native pairing at the beginning of the experiment had been completely compensated. Comparison of the growth reaction norms of the evolving populations over time suggested that this amelioration occurred rapidly: by the tenth transfer, the native and non-native host-symbiont pairings showed equivalent growth responses to light (Welch t test $t(45.96) = -0.26$, $p = 0.80$), in contrast to their substantially different ancestral growth reaction norms observed at the start of the evolution experiment (Welch t test $t(35.79) = 3.59$, $p < 0.001$) ([Figure S3B](#)). These data suggest that newly established partner-switched symbioses can rapidly achieve equivalent growth performance and fitness benefits as the native host-symbiont pairing through compensatory evolution.

Evolved changes in symbiont load regulation and metabolism

To understand the mechanisms of compensatory evolution, we first compared the symbiont load reaction norms of the ancestral and evolved native and non-native pairings ([Figure 3](#)). Both ancestral host-symbiont pairings showed the expected unimodal symbiont load curve with light, albeit with higher symbiont loads for the native compared to the non-native pairing at the

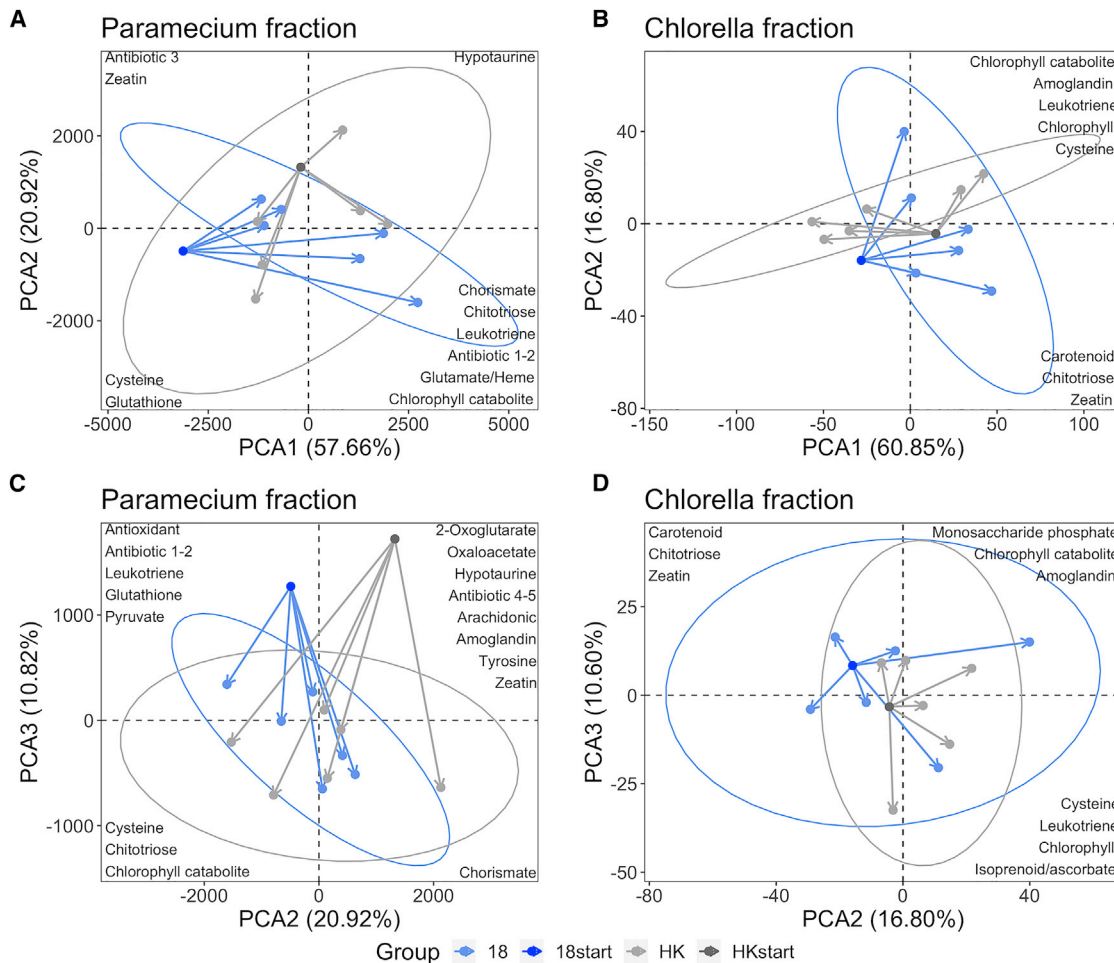


Figure 4. Evolutionary trajectories of *Paramecium* and *Chlorella* metabolism

(A) and (C) show PCA plots for *P. bursaria* metabolism, while (B) and (D) show PCA plots for *Chlorella* metabolism, as indicated in the panel labels. The top row (A and B) plot PC1 versus PC2. The bottom row (C and D) plot PC2 versus PC3. The percentage of variation explained by each PC is shown on the associated axis label. Colors show the symbiont genotype treatment, where blue denotes that the 186b host carried the native 186b symbiont genotype, whereas gray denotes that the 186b host carried the non-native HK1 symbiont genotype. Dark points show ancestral metabolism at the start of the evolution experiment (mean of $n = 6$), whereas light points show the metabolism of each individual replicate population at the end of the evolution experiment (mean of $n = 3$ technical replicates per population). Arrows show the trajectory of metabolic evolution followed by each replicate population during the evolution experiment, and 95% confidence ellipses have been drawn for each treatment. The metabolite identifications for the top loadings are shown in their corresponding location. Related to [Figure S4](#) and [Tables S2](#) and [S3](#).

highest light level, $50 \mu\text{E m}^{-2} \text{s}^{-1}$ irradiance, as used in the transfer experiment. By the end of the evolution experiment, the shape of the symbiont load reaction norms were altered in both the native and non-native pairings. Most notably, at $50 \mu\text{E m}^{-2} \text{s}^{-1}$ irradiance, whereas the non-native pairing had increased symbiont load, symbiont load had decreased in the native pairing, such that symbiont load was now higher in the non-native pairing (transfer by symbiont genotype interaction at high light: ANOVA, $F_{3,20} = 16.88$, $p < 0.001$). Higher symbiont loads may therefore have contributed to the observed increased fitness of evolved compared to ancestral non-native pairings in the high light environment.

Next, to investigate the potential underlying metabolic mechanisms, we performed untargeted metabolomics analyses on the separated *Chlorella* and *P. bursaria* fractions from samples taken the start and end of the evolution experiment grown at

$50 \mu\text{E m}^{-2} \text{s}^{-1}$. The ancestral *P. bursaria* and *Chlorella* metabolic profiles of native and non-native host-symbiont pairings could be clearly distinguished ([Figure 4](#)). At the end of the evolution experiment, *P. bursaria* metabolism displayed a high degree of apparent convergence between hosts evolved with the native versus the non-native symbionts ([Figures 4A](#) and [4C](#)). This was driven by decreased levels of compounds of central metabolism (such as pyruvate and TCA cycle intermediates, antioxidants, lipids, and some amino acids) ([Table S2](#)), suggesting either increased pathway completion or a reduced metabolic rate, both of which can lead to increased efficiency. In addition, we observed increased levels of the amino acid cysteine and a shikimate pathway component in hosts evolved with the native versus the non-native symbionts ([Figure S4](#)). Levels of algal-cell degradation components ([Figure S4](#)), such as cell-wall degradation product chitotriose, were increased in some

replicates of hosts evolved with either symbiont, potentially suggesting increased digestion of *Chlorella*, which is a known mechanism by which hosts control their symbiont load.^{29,30}

In contrast, evolved changes to the metabolic profiles of the algal symbiont genotypes showed less consistent differences among treatments (Figures 4B and 4D). Whereas all replicates of the native 186b *Chlorella* evolved in a similar direction, the replicates of the non-native HK1 *Chlorella* evolved in two different directions. Two of the HK1 replicates took a similar trajectory to the 186b symbionts, while the remaining four replicates all followed an alternative evolutionary trajectory. The group of four HK1 replicates that diverged during the experiment had lower production of metabolites within core aspects of metabolism, such as lipids, amino acids, and carbohydrates. The second group, including the remaining two HK1 replicates and all the 186b replicates, had for the most part higher production of metabolites within primary metabolism pathways, particularly within lipids and carbohydrates, as well as a key chlorophyll compound, a photo-protective carotenoid (though not for all of the 186b replicates), and secondary metabolites with potential antioxidant properties (Figure S4; Table S2). This greater investment into photosynthesis and photo-protection may improve carbon transfer to the host,^{31,32} and decrease light stress, which aligns with the decrease in host antioxidants. Interestingly, the two HK1 replicates that appeared to converge metabolically with the native symbionts had a lower increase in symbiont load compared to the replicates that metabolically diverged (Table S3). This implies that the evolution of metabolism and symbiont load were linked and that overall two alternative strategies of compensatory evolution emerged: either to have fewer, more beneficial symbionts or to have more, less-beneficial symbionts.

DISCUSSION

Partner switching plays an important role in the evolution of a wide range of symbioses^{2,4,5,33,34} enabling adaptation to changing environments and recovery from the breakdown of symbiosis. Because of intergenomic epistasis, partner-switched host-symbiont pairings may possess novel adaptive phenotypes but will sometimes exhibit low fitness associated with mismatches between host and symbiont traits, owing to their lack of recent coevolutionary history.^{14,15,35} In the *Paramecium-Chlorella* symbiosis, low fitness host-symbiont pairings were associated with elevated symbiont stress responses either in dark or high irradiance environments, suggesting that mismatching light management traits between host and symbiont genotypes may be a potential cause of intergenomic epistasis. This corresponds with findings from other photosynthetic symbioses, including coral-*Symbiodinium* and *Hydra-Chlorella*, where mismatching thermal and light stress tolerances contribute to the breakdown of symbiosis.^{36–39} Low fitness, partner-switched host-symbiont pairings were rescued by compensatory evolution, which took one of two routes: either hosts evolved higher symbiont loads to mitigate for their new algal symbiont's poor performance or the algal symbionts themselves evolved higher investment in photosynthesis and photoprotection traits to better mitigate light stress. Given that symbiont load varies with light due to host control,^{24,25} it seems likely that the evolved change in symbiont load is due

to phenotypic plasticity through altered host regulation, whereas the evolved change in algal photosynthetic metabolism could be due to either genetic or physiological adaptation by the symbionts. Both strategies increased growth of the non-native host-symbiont pairing, leading to higher fitness equivalent to that of the native host-symbiont pairing. Together, these data suggest that partner switching combined with rapid compensatory evolution can contribute to the recovery of symbiosis and local adaptation of hosts to changing environmental conditions. Partner switching combined with rapid compensatory evolution could thus enhance the resilience of symbioses to environmental change, enabling the maintenance of their contribution to ecosystem function. Moreover, the potential fitness benefits of the phenotypic plasticity provided by partner switching may select against the evolution of strict vertical transmission in symbioses that inhabit fluctuating or rapidly changing environments.

STAR★METHODS

Detailed methods are provided in the online version of this paper and include the following:

- KEY RESOURCES TABLE
- RESOURCE AVAILABILITY
 - Lead contact
 - Materials availability
 - Data and code availability
- EXPERIMENTAL MODEL AND SUBJECT DETAILS
- METHOD DETAILS
 - Cross infection
 - Diagnostic PCR
 - Growth rate
 - Symbiont load
 - Metabolomics experiment
 - Mass spectrometry
 - Identification of significant masses
 - Evolution experiment
 - Fitness assay
 - Metabolomics
 - Metabolomics analysis
 - Identification of significant masses
- QUANTIFICATION AND STATISTICAL ANALYSIS

SUPPLEMENTAL INFORMATION

Supplemental information can be found online at <https://doi.org/10.1016/j.cub.2021.06.034>.

ACKNOWLEDGMENTS

This work was funded by grants NE/K011774/2 and NE/V000128/1 from the Natural Environment Research Council, UK to M.A.B., D.D.C., and A.J.W. and a White Rose DTP studentship from the Biotechnology and Biological Sciences Research Council, UK (BB/011151/1) to M.E.S.S. The funders had no role in the design of the study, the collection, analysis, and interpretation of data, or writing of the manuscript. We are grateful to Heather Walker for her technical assistance with the mass spectrometry.

AUTHOR CONTRIBUTIONS

M.A.B., D.D.C., and M.E.S.S. conceived and designed the study. M.E.S.S. conducted experimental work. M.E.S.S. and D.D.C. analyzed the data. M.E.S.S. and M.A.B. drafted the manuscript. All authors commented on the manuscript.

DECLARATION OF INTERESTS

The authors declare no competing interests.

Received: February 16, 2021

Revised: April 9, 2021

Accepted: June 10, 2021

Published: July 12, 2021

REFERENCES

1. Sachs, J.L., and Simms, E.L. (2006). Pathways to mutualism breakdown. *Trends Ecol. Evol.* *21*, 585–592.
2. Boulotte, N.M., Dalton, S.J., Carroll, A.G., Harrison, P.L., Putnam, H.M., Peplow, L.M., and van Oppen, M.J. (2016). Exploring the *Symbiodinium* rare biosphere provides evidence for symbiont switching in reef-building corals. *ISME J.* *10*, 2693–2701.
3. Lefèvre, C., Charles, H., Vallier, A., Delobel, B., Farrell, B., and Heddi, A. (2004). Endosymbiont phylogenesis in the dryophthoridae weevils: evidence for bacterial replacement. *Mol. Biol. Evol.* *21*, 965–973.
4. Koga, R., and Moran, N.A. (2014). Swapping symbionts in spittlebugs: evolutionary replacement of a reduced genome symbiont. *ISME J.* *8*, 1237–1246.
5. Matsuura, Y., Moriyama, M., Łukasiak, P., Vanderpool, D., Tanahashi, M., Meng, X.-Y., McCutcheon, J.P., and Fukatsu, T. (2018). Recurrent symbiont recruitment from fungal parasites in cicadas. *Proc. Natl. Acad. Sci. USA* *115*, E5970–E5979.
6. Heath, K.D. (2010). Intergenomic epistasis and coevolutionary constraint in plants and rhizobia. *Evolution* *64*, 1446–1458.
7. Thompson, J.N. (2005). *The Geographic Mosaic of Coevolution* (University of Chicago Press).
8. Heath, K.D., and Tiffin, P. (2007). Context dependence in the coevolution of plant and rhizobial mutualists. *Proc. Biol. Sci.* *274*, 1905–1912.
9. Joy, J.B. (2013). Symbiosis catalyses niche expansion and diversification. *Proc. Biol. Sci.* *280*, 20122820.
10. Sudakran, S., Kost, C., and Kaltenpoth, M. (2017). Symbiont Acquisition and Replacement as a Source of Ecological Innovation. *Trends Microbiol.* *25*, 375–390.
11. Jaenike, J., Unckless, R., Cockburn, S.N., Boelio, L.M., and Perlman, S.J. (2010). Adaptation via symbiosis: recent spread of a *Drosophila* defensive symbiont. *Science* *329*, 212–215.
12. Jiggins, F.M., and Hurst, G.D.D. (2011). *Microbiology*. Rapid insect evolution by symbiont transfer. *Science* *332*, 185–186.
13. Matthews, J.L., Oakley, C.A., Lutz, A., Hillyer, K.E., Roessner, U., Grossman, A.R., Weis, V.M., and Davy, S.K. (2018). Partner switching and metabolic flux in a model cnidarian-dinoflagellate symbiosis. *Proc. Biol. Sci.* *285*, 20182336.
14. Russell, J.A., and Moran, N.A. (2005). Horizontal transfer of bacterial symbionts: heritability and fitness effects in a novel aphid host. *Appl. Environ. Microbiol.* *71*, 7987–7994.
15. McGraw, E.A., Merritt, D.J., Droller, J.N., and O'Neill, S.L. (2002). *Wolbachia* density and virulence attenuation after transfer into a novel host. *Proc. Natl. Acad. Sci. USA* *99*, 2918–2923.
16. Nakayama, S., Parratt, S.R., Hutchence, K.J., Lewis, Z., Price, T.A., and Hurst, G.D.D. (2015). Can maternally inherited endosymbionts adapt to a novel host? Direct costs of *Spiroplasma* infection, but not vertical transmission efficiency, evolve rapidly after horizontal transfer into *D. melanogaster*. *Heredity* *114*, 539–543.
17. Sullivan, J.T., Patrick, H.N., Lowther, W.L., Scott, D.B., and Ronson, C.W. (1995). Nodulating strains of *Rhizobium loti* arise through chromosomal symbiotic gene transfer in the environment. *Proc. Natl. Acad. Sci. USA* *92*, 8985–8989.
18. Johnson, M.D. (2011). The acquisition of phototrophy: adaptive strategies of hosting endosymbionts and organelles. *Photosynth. Res.* *107*, 117–132.
19. Kadono, T., Kawano, T., Hosoya, H., and Kosaka, T. (2004). Flow cytometric studies of the host-regulated cell cycle in algae symbiotic with green paramecium. *Protoplasma* *223*, 133–141.
20. Ziesenisz, E., Reisser, W., and Wiessner, W. (1981). Evidence of de novo synthesis of maltose excreted by the endosymbiotic *Chlorella* from *Paramecium bursaria*. *Planta* *153*, 481–485.
21. Kodama, Y., and Fujishima, M. (2011). Four important cytological events needed to establish endosymbiosis of symbiotic *Chlorella* sp. to the alga-free *Paramecium bursaria*. *Japanese Journal of Protozoology* *44*, 1–20.
22. Siegel, R.W. (1960). Hereditary endosymbiosis in *Paramecium bursaria*. *Exp. Cell Res.* *19*, 239–252.
23. Sørensen, M.E.S., Wood, A.J., Minter, E.J.A., Lowe, C.D., Cameron, D.D., and Brockhurst, M.A. (2020). Comparison of independent evolutionary origins reveals both convergence and divergence in the metabolic mechanisms of symbiosis. *Curr. Biol.* *30*, 328–334.e4.
24. Lowe, C.D., Minter, E.J., Cameron, D.D., and Brockhurst, M.A. (2016). Shining a Light on Exploitative Host Control in a Photosynthetic Endosymbiosis. *Curr. Biol.* *26*, 207–211.
25. Dean, A.D., Minter, E.J.A., Sørensen, M.E.S., Lowe, C.D., Cameron, D.D., Brockhurst, M.A., and Jamie Wood, A. (2016). Host control and nutrient trading in a photosynthetic symbiosis. *J. Theor. Biol.* *405*, 82–93.
26. Minter, E.J.A., Lowe, C.D., Sørensen, M.E.S., Wood, A.J., Cameron, D.D., and Brockhurst, M.A. (2018). Variation and asymmetry in host-symbiont dependence in a microbial symbiosis. *BMC Evol. Biol.* *18*, 108.
27. Mallick, N. (2004). Copper-induced oxidative stress in the chlorophycean microalga *Chlorella vulgaris*: response of the antioxidant system. *J. Plant Physiol.* *161*, 591–597.
28. Shiu, C.-T., and Lee, T.-M. (2005). Ultraviolet-B-induced oxidative stress and responses of the ascorbate-glutathione cycle in a marine macroalga *Ulva fasciata*. *J. Exp. Bot.* *56*, 2851–2865.
29. Kodama, Y., and Fujishima, M. (2008). Cycloheximide induces synchronous swelling of perialgal vacuoles enclosing symbiotic *Chlorella vulgaris* and digestion of the algae in the ciliate *Paramecium bursaria*. *Protist* *159*, 483–494.
30. Kodama, Y., and Fujishima, M. (2012). Cell division and density of symbiotic *Chlorella variabilis* of the ciliate *Paramecium bursaria* is controlled by the host's nutritional conditions during early infection process. *Environ. Microbiol.* *14*, 2800–2811.
31. Cantin, N.E., van Oppen, M.J.H., Willis, B.L., Mieog, J.C., and Negri, A.P. (2009). Juvenile corals can acquire more carbon from high-performance algal symbionts. *Coral Reefs* *28*, 405.
32. Freeman, C.J., Thacker, R.W., Baker, D.M., and Fogel, M.L. (2013). Quality or quantity: is nutrient transfer driven more by symbiont identity and productivity than by symbiont abundance? *ISME J.* *7*, 1116–1125.
33. Husnik, F., and McCutcheon, J.P. (2016). Repeated replacement of an intrabacterial symbiont in the tripartite nested mealybug symbiosis. *Proc. Natl. Acad. Sci. USA* *113*, E5416–E5424.
34. Rolshausen, G., Grande, F.D., Sadowska-Deś, A.D., Otte, J., and Schmitt, I. (2018). Quantifying the climatic niche of symbiont partners in a lichen symbiosis indicates mutualist-mediated niche expansions. *Ecography* *41*, 1380–1392.
35. Matthews, J.L., Oakley, C.A., Lutz, A., Hillyer, K.E., Roessner, U., Grossman, A.R., Weis, V.M., and Davy, S.K. (2018). Partner switching and metabolic flux in a model cnidarian-dinoflagellate symbiosis. *Proc. Biol. Sci.* *285*, 20182336.
36. Weis, V.M. (2008). Cellular mechanisms of Cnidarian bleaching: stress causes the collapse of symbiosis. *J. Exp. Biol.* *211*, 3059–3066.

37. Abrego, D., Ulstrup, K.E., Willis, B.L., and van Oppen, M.J.H. (2008). Species-specific interactions between algal endosymbionts and coral hosts define their bleaching response to heat and light stress. *Proc. Biol. Sci.* 275, 2273–2282.
38. Ye, S., Bhattacharjee, M., and Siemann, E. (2019). Thermal Tolerance in Green Hydra: Identifying the Roles of Algal Endosymbionts and Hosts in a Freshwater Holobiont Under Stress. *Microb. Ecol.* 77, 537–545.
39. Howells, E.J., Beltran, V.H., Larsen, N.W., Bay, L.K., Willis, B.L., and van Oppen, M.J.H. (2012). Coral thermal tolerance shaped by local adaptation of photosymbionts. *Nat. Clim. Chang.* 2, 116–120.
40. Hoshina, R., Kato, Y., Kamako, S., and Imamura, N. (2005). Genetic evidence of “American” and “European” type symbiotic algae of *Paramecium bursaria* Ehrenberg. *Plant Biol.* 7, 526–532.
41. Overy, S.A., Walker, H.J., Malone, S., Howard, T.P., Baxter, C.J., Sweetlove, L.J., Hill, S.A., and Quick, W.P. (2005). Application of metabolite profiling to the identification of traits in a population of tomato introgression lines. *J. Exp. Bot.* 56, 287–296.
42. Schneider, C.A., Rasband, W.S., and Eliceiri, K.W. (2012). NIH Image to ImageJ: 25 years of image analysis. *Nat. Methods* 9, 671–675.
43. Benton, H.P., Want, E.J., and Ebbels, T.M.D. (2010). Correction of mass calibration gaps in liquid chromatography-mass spectrometry metabolomics data. *Bioinformatics* 26, 2488–2489.
44. Smith, C.A., Want, E.J., O’Maille, G., Abagyan, R., and Siuzdak, G. (2006). XCMS: processing mass spectrometry data for metabolite profiling using nonlinear peak alignment, matching, and identification. *Anal. Chem.* 78, 779–787.
45. Tautenhahn, R., Böttcher, C., and Neumann, S. (2008). Highly sensitive feature detection for high resolution LC/MS. *BMC Bioinformatics* 9, 504.
46. Kaefer, A., Lingner, T., Feussner, K., Göbel, C., Feussner, I., and Meinicke, P. (2009). MarVis: a tool for clustering and visualization of metabolic biomarkers. *BMC Bioinformatics* 10, 92.
47. Stein, J.R. (1979). (ED.) *Handbook of Phycological Methods: Culture Methods and Growth Measurements* (Cambridge University Press).
48. Kanehisa, M., and Goto, S. (2000). KEGG: kyoto encyclopedia of genes and genomes. *Nucleic Acids Res.* 28, 27–30.
49. Kanehisa, M., Sato, Y., Furumichi, M., Morishima, K., and Tanabe, M. (2019). New approach for understanding genome variations in KEGG. *Nucleic Acids Res.* 47 (D1), D590–D595.
50. Smith, C.A., O’Maille, G., Want, E.J., Qin, C., Trauger, S.A., Brandon, T.R., Custodio, D.E., Abagyan, R., and Siuzdak, G. (2005). METLIN: a metabolite mass spectral database. *Ther. Drug Monit.* 27, 747–751.
51. Lenski, R.E., Rose, M.R., Simpson, S.C., and Tadler, S.C. (1991). Long-Term Experimental Evolution in *Escherichia coli*. I. Adaptation and Divergence During 2,000 Generations. *Am. Nat.* 138, 1315–1341.
52. Warnes, G.R., Bolker, B., Bonebakker, L., Gentleman, R., Huber, W., Liaw, A., Lumley, T., Maechler, M., Magnusson, A., and Moeller, S. (2009). ggplots: Various R programming tools for plotting data (R package version 2, 1).
53. Cotton, T.E.A., Pétriacq, P., Cameron, D.D., Meselmani, M.A., Schwarzenbacher, R., Rolfe, S.A., and Ton, J. (2019). Metabolic regulation of the maize rhizobiome by benzoxazinoids. *ISME J.* 13, 1647–1658.
54. Caspi, R., Billington, R., Fulcher, C.A., Keseler, I.M., Kothari, A., Krummenacker, M., Latendresse, M., Midford, P.E., Ong, Q., Ong, W.K., et al. (2018). The MetaCyc database of metabolic pathways and enzymes. *Nucleic Acids Res.* 46 (D1), D633–D639.
55. R Core Team (2018). R: A Language and Environment for Statistical Computing.
56. Wickham, H. (2016). ggplot2: Elegant Graphics for Data Analysis.
57. Pinheiro, J., Bates, D., DebRoy, S., and Sarkar, D.; R core Team (2019). nlme: Linear and Nonlinear Mixed Effects Models.

STAR★METHODS

KEY RESOURCES TABLE

REAGENT or RESOURCE	SOURCE	IDENTIFIER
Bacterial and virus strains		
<i>Serratia marcescens</i>	Collection of Institut Pasteur	Strain ID: CIP 103235T
Chemicals, peptides, and recombinant proteins		
Protozoan Pellet Media	Carolina Biological Supply	Catalog number: 132360
Paraquat dichloride	Sigma-Aldrich	Catalog number: 36541; CAS: 75365-73-0
8-peak rainbow calibration particles	BioLegend	Catalog number: 422903
Chelex100 resin	Bio-Rad Laboratories	Catalog number: 1421253
Deposited data		
Mass spectrometry, growth rate, fitness assays and flow cytometry data	This paper	https://doi.org/10.17632/m7tpztyjx.1
Experimental models: organisms/strains		
<i>P. bursaria</i> – <i>Chlorella</i> 186b strain	Culture Collection of Algae and Protozoa	Strain ID: CCAP 1660/18
<i>P. bursaria</i> – <i>Chlorella</i> HA1 strain	National BioResource project	Strain ID: NBRP PB034004A
<i>P. bursaria</i> – <i>Chlorella</i> HK1 strain	National BioResource project	Strain ID: NBRP PB033003A
Oligonucleotides		
primer 'SR1' (F): TACCTGGTTGATCCTGCCAG	Hoshina et al. ⁴⁰	N/A
Primer 'CHspeRmaeF' (F): GGCCTTTTCAGGTCTGGTA	Hoshina et al. ⁴⁰	N/A
Primer 'INT4F': TGGTGAAGTGTTCCGATTGG	Hoshina et al. ⁴⁰	N/A
Primer 'SR8' (F): GGATTGACAGATTGAGAGCT	Hoshina et al. ⁴⁰	N/A
Primer 'chSsotoR': CCCTAAGAAGTCCGCCG	Hoshina et al. ⁴⁰	N/A
Primer 'INT5R': AGGTGGGAGGGTTAATGAA	Hoshina et al. ⁴⁰	N/A
Primer 'HLR3R': TCCCAAACAACCCGACTCT	Hoshina et al. ⁴⁰	N/A
Primer 'TreSR': GCCAGTGCACACCGAAAC	Hoshina et al. ⁴⁰	N/A
Primer 'CHspeHLR1R': CACTAGACTACAATTCGCCAGCC	Hoshina et al. ⁴⁰	N/A
Software and algorithms		
Visual Basic macro 216	Overy et al. ⁴¹	https://pubmed.ncbi.nlm.nih.gov/15596481/
ImageJ v1.50i	Schneider et al. ⁴²	https://imagej.nih.gov/ij/
xcms R package	Benton et al., ⁴³ Smith et al., ⁴⁴ Tautenhahn et al. ⁴⁵	https://bioconductor.org/packages/release/bioc/html/xcms.html
MarVis-Suite 2.0 software	Kaever et al. ⁴⁶	http://marvis.gobics.de/

RESOURCE AVAILABILITY

Lead contact

Further information and requests for resources and reagents should be directed to and will be fulfilled by the Lead Contact, Michael Brockhurst (michael.brockhurst@manchester.ac.uk).

Materials availability

The natural strains used in this paper are available from culture collections (see below), unfortunately all our experimental populations were lost during the lab closures at the beginning of the global Covid pandemic.

Data and code availability

The data has been deposited within Mendeley Data (Mendeley Data: <https://doi.org/10.17632/m7tpztyjx.1>).

EXPERIMENTAL MODEL AND SUBJECT DETAILS

The three natural strains of symbiotic *P. bursaria* used were: 186b (CCAP 1660/18) obtained from the Culture Collection for Algae and Protozoa (Oban, Scotland), and HA1 and HK1 isolated in Japan and obtained from the Paramecium National Bio-Resource Project (Yamaguchi, Japan). *P. bursaria* stock cultures were maintained at 25°C under a 14:10 L:D cycle with 50 $\mu\text{E m}^{-2} \text{s}^{-1}$ of light (a high light condition). The stocks were maintained by batch culture in bacterized Protozoan Pellet Media (PPM, Carolina Biological Supply), made to a concentration of 0.66 g L⁻¹ with Volvic natural mineral water, and inoculated approximately 20 hours prior to use with *Serratia marcescens* from frozen glycerol stocks.

To isolate *Chlorella* from the symbiosis, symbiotic cultures were first washed and concentrated with a 11 μm nylon mesh using sterile Volvic. The suspension was then ultrasonicated using a Fisherbrand Q500 Sonicator (Fisher Scientific, NH, USA), at a power setting of 20% for 10 s sonification to disrupt the host cells. The liquid was then spotted onto Bold Basal Media plates (BBM)⁴⁷, from which green colonies were streaked out and isolated over several weeks. Plate stocks were maintained by streaking out one colony to a fresh plate every 3/4 weeks.

Symbiont-free *P. bursaria* were made by treating symbiotic cultures with paraquat (10 $\mu\text{g mL}^{-1}$) for 3 to 7 days in high light conditions ($> 50 \mu\text{E m}^{-2} \text{s}^{-1}$), until the host cells were visibly symbiont free. The cultures were then extensively washed with Volvic and closely monitored with microscopy and flow cytometry over a period of several weeks to check that re-greening by *Chlorella* did not occur. Stock cultures of the symbiont-free cells were maintained by batch culture at 25°C under a 14:10 L:D cycle with 3 $\mu\text{E m}^{-2} \text{s}^{-1}$ of light and were given fresh PPM weekly. Symbiont-free *Paramecium* stocks have been maintained for a substantial period of time (months/years) without *Chlorella* ever being observed either inside or outside of *Paramecium* cells. In addition, using flow cytometry we have never observed chlorophyll fluorescence for *Paramecium* cells sampled from these stocks (methodology detailed in symbiont Load section). Together these tests confirm that paraquat treatment successfully removes all of the native *Chlorella*.

METHOD DETAILS

Cross infection

Symbiont-free populations of the three *P. bursaria* strains were re-infected by adding a colony of *Chlorella* from the plate stocks derived from the appropriate strain. This was done with all three of the isolated *Chlorella* strains to construct all possible host-symbiont genotype pairings ($n = 9$). The regreening process was followed by microscopy and took between 2-6 weeks. Over the process, cells were grown at the intermediate light level of 12 $\mu\text{E m}^{-2} \text{s}^{-1}$ and were given bacterized PPM weekly.

Diagnostic PCR

The correct algae genotype within the cross-infections was confirmed using diagnostic PCR. The *Chlorella* DNA was extracted by isolating the *Chlorella* and then using a standard 6% Chelex100 resin (Bio-Rad) extraction method. A nested PCR technique with overlapping, multiplex Chlorophyta specific primers were used as described by Hoshina et al.⁴⁰. Standard PCR reactions were performed using Go Taq Green Master Mix (Promega) and 0.5 $\mu\text{mol L}^{-1}$ of the primer. The thermocycler program was set to: 94°C for 5 min, 30 cycles of (94°C for 30 sec, 55°C for 30 sec, 72°C for 60 sec), and 5 min at 72°C.

Growth rate

Growth rates of the host-symbiont pairings were measured across a light gradient. The cells were washed and concentrated with a 11 μm nylon mesh using sterile Volvic and re-suspended in bacterized PPM. The cultures were then split and acclimated to their treatment light condition (0, 12, 24, & 50 $\mu\text{E m}^{-2} \text{s}^{-1}$) for five days. The cultures were then re-suspended in bacterized PPM to a target cell density of 150 cell mL⁻¹. Cell densities were measured at 0, 24, 48 and 72 hours by fixing 360 μL of each cell culture, in triplicate, in 1% v/v glutaraldehyde in 96-well flat-bottomed micro-well plates. Images were taken with a plate reader (Tecan Spark 10M) and cell counts were made using an automated image analysis macro in ImageJ v1.50i⁴². The initial host-symbiont growth rate was measured over a period of three days.

Symbiont load

The symbiont load (i.e., the number of symbionts per host cell) was measured in cultures derived from the growth rate experiment so that the data could be integrated between the two measurements. Triplicate 300 μL samples of each cell culture were taken from 72-hour cultures for flow cytometry analysis. Host symbiont load was estimated using a CytoFLEX S flow cytometer (Beckman Coulter Inc., CA, USA) by measuring the intensity of chlorophyll fluorescence for single *P. bursaria* cells (excitation 488nm, emission 690/50nm) and gating cell size using forward side scatter; a method established by Kadono et al.¹⁹. The measurements were calibrated

against 8-peak rainbow calibration particles (BioLegend), and then presented as relative fluorescence to reduce variation across sampling sessions.

Metabolomics experiment

Cultures of the host-symbiont pairings were washed and concentrated with a 11 μm nylon mesh using sterile Volvic and re-suspended in bacterized PPM. The cultures were then split and acclimated at their treatment light condition (0, 12 & 50 $\mu\text{E m}^{-2} \text{s}^{-1}$) for seven days. The symbiotic partners were separated in order to get *P. bursaria* and *Chlorella* metabolic fraction. The *P. bursaria* cells were concentrated with a 11 μm nylon mesh using Volvic and then the *P. bursaria* cells were disrupted by sonication (20% power for 10 s). 1 ml of the lysate was pushed through a 1.6 μm filter, which caught the intact *Chlorella* cells, and the run-through was collected and stored as the *P. bursaria* fraction. The 1.6 μm filter was washed with 5 ml cold deionized water, and then reversed so that the *Chlorella* cells were resuspended in 1 ml of cold methanol, which was stored as the *Chlorella* fraction. After which the *Chlorella* fraction samples were already in methanol, but the *P. bursaria* fraction samples had then to be diluted by 50% with methanol.

Mass spectrometry

Metabolic profiles were recorded using ESI ToF-MS, on the Qstar Elite with automatic injection using Waters Alliance 2695 HPLC (no column used), in positive mode. This is an established high-throughput method with a large mass range (50 Da to 1000 Da).

The mass spectrometry settings were: positive polarity, 4.2 kV Ion Spray voltage, 120 V Declustering potential, 265 V Focusing potential, 200 °C Source temperature, 40 mL min^{-1} Gas Flow, the solvent was 50:50 methanol to water at flow rate 40 $\mu\text{L min}^{-1}$ and the injected volume was 10 μL .

The processing was performed using in-house software Visual Basic macro 216⁴¹, which combined the spectra across the technical replicates by binning the crude m/z values into 0.2-unit bins. The relative mass abundances (% total ion count) for each bin was summed. Pareto scaling was applied to the results, and the data was then analyzed by principal component analysis using SIMCA-P software (Umetrics). When treatment-based separation was observed, supervised orthogonal partial least-squares discriminant analysis (OPLS-DA) separation was then performed using the discriminatory treatment with the SIMCA-P software.

Identification of significant masses

Masses of interest were annotated using the initial identifications from the in-house software program and further comparisons against KEGG (<https://www.genome.jp/kegg/>)^{48,49} and Metlin (<https://metlin.scripps.edu>)⁵⁰ databases. The Metabolomics Standards Initiative requires two independent measures to confirm identity, this partner-switching metabolomic analysis only used one measure (accurate mass) and therefore, meets only the level 2 requirements of putative annotated compounds.

Evolution experiment

The populations used derive from the cross-infections and, therefore, the host-symbiont pairings come from the same cured 186b ancestor that was then re-infected with either its native (186b) or non-native (HK1) symbionts. The two host-symbiont pairings were split into six replicate populations that were used as the starting populations. The 200 ml populations were propagated by weekly serial transfer for 25 transfers at a high light (50 $\mu\text{E m}^{-2} \text{s}^{-1}$) 14:10 L:D cycle. At every transfer, cell-density was equalised to 100 cells mL^{-1} and the transferred cells were washed with a 11 μm nylon mesh using Volvic before being re-suspended in bacterized PPM. Cell density was measured before and after each transfer by fixing 360 μL of each cell culture, in triplicate, in 1% v/v glutaraldehyde in 96-well flat-bottomed micro-well plates. Images were taken with a plate reader (Tecan Spark 10M) and cell counts were made using an automated image analysis macro in ImageJ v1.50i⁴². Growth rate and symbiont load assays were conducted at the start, T10, T20 and end of the experiment using the method described above.

Fitness assay

Fitness assays were conducted at the start and end of the evolution experiment. *P. bursaria* cultures, both the symbiotic pairings and the symbiont-free ancestor, were washed with Volvic and resuspended in bacterized PPM. The cultures were then split and acclimated at their treatment light level (0, 12, 50 $\mu\text{E m}^{-2} \text{s}^{-1}$) for five days. Cell densities were counted by fixing 360 μL of each cell culture, in triplicate, in 1% v/v glutaraldehyde in 96-well flat-bottomed micro-well plates. Images were taken with a plate reader (Tecan Spark 10M) and cell counts were made using an automated image analysis macro in ImageJ v1.50i⁴². The competitions were started by setting up microcosms that each contained 50:50 populations of green and white cells (with target values of 20 green cells and 20 white cells per mL) that were in direct competition. Cells were sampled on day 0 and day 7 on a flow cytometer and the proportion of green to white cells was measured and used to calculate the selection rate. Selection rate (R) is calculated as the difference in Malthusian parameters of green (test) versus white (reference) cell populations in direct competition: $R = (\ln(\text{test}_{\text{start}}/\text{test}_{\text{end}}) - \ln(\text{reference}_{\text{start}}/\text{reference}_{\text{end}})) / \text{day}$ ⁵¹. Green versus white cells were distinguished using single cell fluorescence estimated using a CytOFLEX S flow cytometer (Beckman Coulter Inc., CA, USA) by measuring the intensity of chlorophyll fluorescence (excitation 488 nm, emission 690/50 nm) and gating cell size using forward side scatter; a method established by Kadono et al.¹⁹. The measurements were calibrated against 8-peak rainbow calibration particles (BioLegend), and then presented as relative fluorescence to reduce variation across sampling sessions. The re-establishment of endosymbiosis takes between 2–4 weeks, and this method was tested to ensure that the symbiont-free cells do not re-green over the course of the experiment.

Metabolomics

The cultures were sampled at the start and end of the evolution experiment. Cultures were washed and concentrated with a 11 μm nylon mesh using Volvic and re-suspended in bacterized PPM. The cultures were acclimated at their treatment light condition ($50 \mu\text{E m}^{-2} \text{s}^{-1}$) for seven days. At the start of the evolution experiment we analyzed a sample from each of the 6 replicate populations per treatment to determine the ancestral metabolomes of each host-symbiont pairing (i.e., $n = 6$). At the end of the evolution experiment, we increased our replication such that for each of the 6 replicate populations per treatment we analyzed 3 technical replicates, allowing us to determine differences between replicate populations as well as between treatments in their evolved metabolomes. At each sampling event, the symbiotic partners were separated in order to get *P. bursaria* and *Chlorella* metabolic fraction using the extraction method described above. Samples were freeze-dried for storage, and then resuspended in 50:50 methanol to water prior to mass spectrometry.

The samples were analyzed with a Synapt G2-Si with Acuity UPLC, recording in positive mode over a large untargeted mass range (50 – 1000 Da). A 2.1x50mm Acuity UPLC BEH C18 column was used with acetonitrile as the solvent. The machine settings are listed in detail below:

The mass spectrometry settings were: positive polarity, 2.3kV Capillary voltage, 20V Sample Cone voltage, 100c Source Temperature, 280c Desolvation temperature, 600 L hr⁻¹ Gas Flow, 5 μL Injected volume and 45c Column temperature. The gradient started at time 0 with 95% water to 5% acetonitrile, at 3 minutes it was 65% water to 35% acetonitrile, at 6 minutes it was 0% water to 100% acetonitrile, at 7.5 minutes it was 0% water to 100% acetonitrile, and at 7.6 minutes it was 95% water to 5% acetonitrile.

The *P. bursaria* and *Chlorella* fraction were analyzed separately. The xcms R package^{43–45} was used to extract the spectra from the CDF data files, using a step argument of 0.01 m/z. Peaks were identified, and then grouped across samples. These aligned peaks were used to identify and correct correlated drifts in retention time from run to run. Pareto scaling was applied to the resulting intensity matrix.

Metabolomics analysis

The metabolic profiles from the start and end of the experiment were compared using principal component analysis (PCA) with the `prcomp()` function in Base R (<http://www.rproject.org/>). For both fractions the first three components were considered, this accounted for > 88% of the variance. The top 1% of the loadings were selected using the absolute magnitude of the loadings. These top loadings were identified where possible, and the identified loadings were then depicted in their associated component space. The relative abundance of these top loadings was visualized using heatmaps drawn with the `heatmap.2()` function from the `gplot` package⁵². The phylogenies were based on UPGMA clustering of the PCA coordinates of the samples using the `hclust()` function. This approach of integrating metabolic data and genotypes in heatmaps has been used previously⁵³.

Identification of significant masses

Masses of interest were investigated using the MarVis-Suite 2.0 software (<http://marvis.gobics.de/>)⁴⁶, using retention time and mass to compare against KEGG (<https://www.genome.jp/kegg/>)^{48,49} and MetaCyc (<https://biocyc.org/>)⁵⁴ databases. The Metabolomics Standards Initiative requires two independent measures to confirm identity, which the combination of retention time and accurate mass achieves for the analysis of the evolution experiment metabolomics.

QUANTIFICATION AND STATISTICAL ANALYSIS

Statistical analyses were performed in Rv.3.5.0⁵⁵ and all plots were produced using package `ggplot2`⁵⁶ unless otherwise stated. Physiology tests were analyzed by both ANOVA and ANCOVA, with transfer time, host and symbiont identity as factors. A linear mixed effect model was used to analysis the growth rate per transfer using `lm()` function from the `nlme` package⁵⁷. The `lm` model included fixed effects of symbiont genotype and transfer number, and random effects of transfer number given sample ID. Where parametric tests were used the data conformed to parametric assumptions of independence, normality and homogeneity of variance, which was confirmed using the appropriate tests and plots (e.g normal QQ and residual versus fitted values). Summary details of the data is provided in the figure legends (e.g the value of n and type of error used) and details of the statistical methods used are within the supplementary statistics data (Data S1).

Within all of our experiments the spatial arrangement of cultures in the incubator was fully randomized to ensure statistical independence. For the short term assays the spatial randomization was reassigned every day. For the long-term evolution experiment the spatial randomization was reassigned at each weekly serial transfer.